Alterations in ether lipid metabolism and the consequences for the mouse lipidome

Lackner, K.; Sailer, S.; Klinken, J.B. van; Wever, E.; Pras-Raves, M.L.; Dane, A.D.; ... ; Watschinger, K.

BBA - Molecular and Cell Biology of Lipids 1868 (2023) 159285

Contents lists available at ScienceDirect

BBA - Molecular and Cell Biology of Lipids

journal homepage: www.elsevier.com/locate/bbalip

Alterations in ether lipid metabolism and the consequences for the mouse lipidome

Katharina Lackner [a], Sabrina Sailer [a,b], Jan-Bert van Klinken [c,d,e], Eric Wever [c,d,f], Mia L. Pras-Raves [c,d,f], Adrie D. Dane [c,f], Masanori Honsho [g], Yuichi Abe [h], Markus A. Keller [b], Georg Golderer [a], Gabriele Werner-Felmayer [a], Yukio Fujiki [i,j], Frédéric M. Vaz [c,d,k], Ernst R. Werner [a], Katrin Watschinger [a,*]

[a] Institute of Biological Chemistry, Biocenter, Medical University of Innsbruck, Innrain 80, 6020 Innsbruck, Austria
[b] Institute of Human Genetics, Medical University of Innsbruck, Peter-Mayr-Strasse 1, 6020 Innsbruck, Austria
[c] Amsterdam UMC location University of Amsterdam, Department of Clinical Chemistry and Pediatrics, Laboratory Genetic Metabolic Diseases, Emma Children's Hospital, Meibergdreef 9, Amsterdam, 1105, AZ, the Netherlands
[d] Core Facility Metabolomics, Amsterdam UMC location University of Amsterdam, Meibergdreef 9, Amsterdam, 1105, AZ, the Netherlands
[e] Department of Human Genetics, Leiden University Medical Center (LUMC), Einthovenweg 20, Leiden, 2333, ZC, the Netherlands
[f] Bioinformatics Laboratory, Department of Epidemiology & Data Science, Amsterdam Public Health Research Institute, Amsterdam UMC location University of Amsterdam, Meibergdreef 9, Amsterdam, 1105, AZ, the Netherlands
[g] Department of Neuroinflammation and Brain Fatigue Science, Graduate School of Medical Sciences, Kyushu University, 3-1-1 Maidashi, Fukuoka 812-8582, Japan
[h] Faculty of Arts and Science, Kyushu University, 744 Motooka, Fukuoka 819-0395, Japan
[i] Institute of Rheological Functions of Food, Kyushu University Collaboration Program, Kyushu University, 3-1-1 Maidashi, Fukuoka 812-8582, Japan
[j] Graduate School of Science, University of Hyogo, Hyogo, Japan
[k] Amsterdam Gastroenterology Endocrinology Metabolism, Inborn Errors of Metabolism, Amsterdam UMC location University of Amsterdam, Meibergdreef 9, Amsterdam 1105, AZ, The Netherlands

ARTICLE INFO

Keywords:
Knockout mouse models
Glycerolipids
Glycerophospholipids
Lipidomics
Plasmalogens
Phospholipids

ABSTRACT

Alkylglycerol monooxygenase (AGMO) and plasmanylethanolamine desaturase (PEDS1) are enzymes involved in ether lipid metabolism. While AGMO degrades plasmanyl lipids by oxidative cleavage of the ether bond, PEDS1 exclusively synthesizes a specific subclass of ether lipids, the plasmalogens, by introducing a vinyl ether double bond into plasmanylethanolamine phospholipids. Ether lipids are characterized by an ether linkage at the *sn*-1 position of the glycerol backbone and they are found in membranes of different cell types. Decreased plasmalogen levels have been associated with neurological diseases like Alzheimer's disease. *Agmo*-deficient mice do not present an obvious phenotype under unchallenged conditions. In contrast, *Peds1* knockout mice display a growth phenotype. To investigate the molecular consequences of *Agmo* and *Peds1* deficiency on the mouse lipidome, five tissues from each mouse model were isolated and subjected to high resolution mass spectrometry allowing the characterization of up to 2013 lipid species from 42 lipid subclasses. *Agmo* knockout mice moderately accumulated plasmanyl and plasmenyl lipid species. *Peds1*-deficient mice manifested striking changes characterized

Abbreviations: AGMO, alkylglycerol monooxygenase; AGPS, alkylglycerone phosphate synthase; BMP, lysobisphosphatidic acid/bis(monoacylglycero)phosphate; CL, cardiolipin; DG, diacylglycerol; DG[O]/[P], plasmanyl/plasmenyl diacylglycerol; DLCL, dilysocardiolipin; FAR1, fatty acyl-CoA reductase 1; GNPAT, glyceronephosphate *O*-acyltransferase; LPA, lysophosphatidic acid; LPA[O + P], plasmanyl and plasmenyl lysophosphatidic acid; LPC, lysophosphatidylcholine; LPC[O]/[P], plasmanyl/plasmenyl lysophosphatidylcholine; LPE, lysophosphatidylethanolamine; LPE[O]/[P], plasmanyl/plasmenyl lysophosphatidylethanolamine; MG, monoacylglycerol; MG[O]/[P], plasmanyl/plasmenyl monoacylglycerol; PA, phosphatidic acid; PA[O + P], plasmanyl and plasmenyl phosphatidic acid; PC, phosphatidylcholine; PC[O]/[P], plasmanyl/plasmenyl phosphatidylcholine; PE, phosphatidylethanolmanine; PE[O]/[P], plasmanyl/plasmenyl phosphatidylethanolamine; PEDS1, plasmanylethanolamine desaturase; PS, phosphatidylserine; sWAT, subcutaneous white adipose tissue; TG, triacylglycerol; TG[O + P], plasmanyl and plasmenyl triacylglycerol; vWAT, visceral white adipose tissue..

* Corresponding author.
E-mail addresses: katharina.lackner@i-med.ac.at (K. Lackner), sabrina.sailer@i-med.ac.at (S. Sailer), j.b.vanklinken@amsterdamumc.nl (J.-B. van Klinken), eric.wever@amsterdamumc.nl (E. Wever), m.pras@amsterdamumc.nl (M.L. Pras-Raves), a.d.dane@amsterdamumc.nl (A.D. Dane), honsho.masanori.707@m.kyushu-u.ac.jp (M. Honsho), y-abe@bio.sojo-u.ac.jp (Y. Abe), markus.keller@i-med.ac.at (M.A. Keller), georg.golderer@i-med.ac.at (G. Golderer), gabriele.werner-felmayer@i-med.ac.at (G. Werner-Felmayer), yfujiki@kyudai.jp (Y. Fujiki), f.m.vaz@amsterdamumc.nl (F.M. Vaz), ernst.r.werner@i-med.ac.at (E.R. Werner), katrin.watschinger@i-med.ac.at (K. Watschinger).

https://doi.org/10.1016/j.bbalip.2023.159285
Received 13 September 2022; Received in revised form 18 December 2022; Accepted 16 January 2023
Available online 21 January 2023

by a strong reduction of plasmenyl lipids and a concomitant massive accumulation of plasmanyl lipids resulting in increased total ether lipid levels in the analyzed tissues except for the class of phosphatidylethanolamines where total levels remained remarkably constant also in *Peds1* knockout mice. The rate-limiting enzyme in ether lipid metabolism, FAR1, was not upregulated in *Peds1*-deficient mice, indicating that the selective loss of plasmalogens is not sufficient to activate the feedback mechanism observed in total ether lipid deficiency.

1. Introduction

Lipids are a multifaceted group of molecules with diverse cellular functions including energy storage, signaling as well as being important membrane components. Investigating lipid homeostasis is crucial for understanding the pathogenesis of lipid defects associated with several diseases. This has been facilitated over the last decades by efforts to improve lipidomics technologies providing researchers nowadays with a multitude of tools to analyze the various lipid classes [1].

One class of lipids, which is comparatively less well studied, are ether lipids. These lipids are characterized by an ether bond at the *sn-1* position of the glycerol backbone, in contrast to classical acylglycerolipids and glycerophospholipids, in which an ester bond is present instead. Ether lipids appear in two forms, 1-*O*-alkyl (plasmanyl) and 1-*O*-alk-1′-enyl (plasmenyl) ether lipids, the latter being also called plasmalogens. Plasmalogens make up around 20 % of the total phospholipid pool in mammals [2]. Highest levels are found in cell membranes of the central nervous system, kidney, heart, lung and immune cells [2,3]. In vitro studies showed that plasmanyl lipids are involved in cellular signal transduction e.g. platelet-activating factor (PAF) was shown to play a role in several pro-inflammatory reactions as well as neuronal functions and reproduction [4]. Additionally, alkylglycerols were linked to the activation of macrophages leading to phagocytosis and increased humoral immune response [5]. Lately, reduced plasmalogen levels were associated with neurodegenerative disorders such as Alzheimer's disease and autism [6] although it is unclear if these changes in the amounts of ether lipids are cause or consequence of the diseases.

The initial steps of ether lipid biosynthesis take place in the peroxisomes and are catalyzed by the enzymes glyceronephosphate O-acyltransferase (GNPAT) and alkylglycerone phosphate synthase (AGPS). Availability of the fatty alcohol needed by AGPS to introduce the ether bond is controlled by fatty acyl-CoA reductase 1 (FAR1). FAR1 is the rate-limiting enzyme of peroxisomal ether lipid biosynthesis and is subjected to degradation upon sensing high levels of plasmalogens [7]. In particular, plasmenylethanolamine (PE[P]) was found to elicit a feedback inhibition, an effect that was not shown by phosphatidylethanolamine (PE) [7]. Rare inherited mutations in FAR1 inactivating this feedback mechanism have been shown to lead to an uncontrolled overproduction of ether lipids resulting in a neurological disorder [8]. Impairment of the initial steps of ether lipid biosynthesis in the rare inherited diseases rhizomelic chondrodysplasia punctata (RCDP) types 1 to 5 and in peroxisome biogenesis disorders of the Zellweger spectrum, lead to severe multisystem pathologies in humans [3]. From the symptoms detected in the affected children it has been deduced what functions plasmanyl and plasmenyl lipids have in the body e.g. protection from infections and cataract as well as maintaining fertility, normal growth and neurodevelopment. Also several mouse models have been created with deficiencies in these peroxisomal genes leading to a total lack of ether lipids. These mice present with growth retardation and cataracts amongst many other deficits [9–11], symptoms that closely mimic the human pathology but, depending on the mouse strain, are usually milder than in humans where most affected children die in early childhood [12].

The final steps of ether lipid remodeling as well as their degradation occur at the endoplasmic reticulum where alkylglycerol monooxygenase (AGMO, E.C. 1.14.16.5) catabolizes plasmanyl lipids [13] or where they are further converted to plasmenyl lipids by the enzyme plasmanylethanolamine desaturase (PEDS1, E.C. 1.14.19.77) [14], which introduces the characteristic 1′ vinyl ether double bond.

AGMO is the only known enzyme so far capable of cleaving alkylglycerols and lysoalkylglycerophospholipids into the corresponding glycerol derivative and a fatty aldehyde. After the first description of the enzymatic reaction in 1964 [15] it took almost 50 years to decipher the genetic sequence coding for AGMO. In 2010, the gene *Tmem195* was assigned to AGMO by a combination of bioinformatic approaches and in vitro expression studies in cell lines [13] using a fluorescence-based HPLC assay to measure AGMO activity [16]. In a follow up study crucial amino acid residues for catalytic activity in AGMO were determined [17]. It was shown that AGMO is differentially regulated upon macrophage polarization and that *Agmo* knockdown in RAW264.7 macrophages alters the cellular lipidome by affecting not only ether lipids but also glycosylated ceramides and cardiolipins [18]. Genetic association studies in humans pointed towards involvement of AGMO in visceral leishmaniasis relapses [19], microcephaly [20,21], autism [22] and congenital heart disease [23,24]. Recently, a knockout mouse model for *Agmo* was established in our laboratory [25]. These mice present with no detectable phenotype when kept in an unchallenged environment [25].

The gene coding for PEDS1 was recently identified as *Tmem189* independently by us and two other groups [14,26,27]. In contrast to AGMO, a *Tmem189*-deficient knockout mouse model was already available from the European Mouse Mutant Archive (EMMA) [28–31]. Characterization of these mice by a standardized protocol of the International Mouse Phenotyping Consortium identified abnormalities in the eyes, the skeletal and hematopoietic system and reduced lean body mass [32]. In addition, we could show that homozygous pups of *Tmem189* knockout mice have severely diminished plasmalogen levels and displayed significantly lower body weight at the time of weaning compared to wildtype littermates [14]. This mouse model was an indispensable tool enabling to establish an LC–MS/MS-based approach to distinguish between isobaric plasmanyl and plasmenyl glycerophospholipids for which the discrimination has been a major analytical challenge in the past years [33]. This MS method also revealed that *Peds1* deficiency leads to concomitant accumulation of ether-linked phosphatidylethanolamine species, the direct substrates of PEDS1, in the kidney [33].

In order to further characterize the impact of *Agmo* and *Peds1* knockout on the murine lipidome and to understand the molecular basis of why *Peds1*-deficient mice present with a distinct phenotype while *Agmo*-deficient mice appear entirely unaffected at least under normal housing conditions, we analyzed the lipid composition in five selected tissues per mouse model using high-resolution mass spectrometry (MS). The consequences of global ether lipid deficiency have long been characterized in mice [12] and were shown to positively feedback to FAR1 protein levels [7]. Yet, little is known about the consequences of selective deficiency in ether lipid metabolism outside the peroxisome.

Here, we report that *Agmo*-deficient mice moderately accumulated plasmanyl and plasmenyl lipid species. *Peds1*-deficient mice, in contrast, were characterized by a strong decrease of plasmalogens paralleled by an even more dramatic increase in the levels of plasmanyl lipids which was found not only in many classes of glycerophospholipids but also in neutral ether lipids leading to an overall accumulation of ether lipids. In the class of phosphatidylethanolamines (PE), however, the amount of plasmanylethanolamines (PE[O]) accumulating in *Peds1*-deficient mice mirrored the observed decrease in the amount of plasmenylethanolamines (PE[P]) leading to constant overall PE levels. *Peds1-deficient* mice showed unchanged FAR1 protein expression in cerebral cortex

revealing that selective loss of plasmalogens and concomitant accumulation of plasmanyl lipids is not sufficient to induce FAR1 levels.

2. Material and methods

2.1. Knockout mouse lines and breeding

Agmo-deficient mice (official line name: *Agmo*$^{tm1a(EUCOMM)Wtsi}$) were generated from embryonic stem cells (clone EPD0354_2_F05, EuMMCR, Munich, Germany) and were maintained on C57BL/6J background (for details see [25]).

Peds1-deficient mice (official line name: *Tmem189*$^{tm1a(KOMP)Wtsi}$) were obtained from the Wellcome Sanger Institute (Hinxton, Cambridge, UK) and the European Mouse Mutant Archive EMMA/Infrafrontier GmbH (Munich, Germany) [28–31] and were maintained on C57bl/6 N genetic background.

Mice were housed in individually ventilated cages with nesting material, in a 12 h/12 h light/dark cycle with standard chow (Ssniff Spezialdiäten GmbH, Soest, Germany; complete feed for rats and mice V1534-300, autoclaved) and water ad libitum. Animal breeding of both mouse lines was approved by the Austrian Federal Ministry of Education, Science and Research (*Agmo*: BMWFW-66.011/0094-WF/V/3b/2016 and BMWFW-66.011/0020-V/3b/2019; *Peds1*: BMBWF-66.011/0100-V/3b/2019).

2.2. Mouse genotyping

Genomic DNA of *Agmo*- and *Peds1*-deficient mice was extracted from ear notches using the Monarch® Genomic DNA Purification Kit (New England Biolabs, Frankfurt am Main, Germany). Genotyping of *Agmo*-deficient mice was done by allele counting via qPCR using SsoFast EvaGreen Supermix (Bio-Rad Laboratories Inc., Hercules, USA) and primers for *Agmo*-lacZ (fw 5′-TCTGTATGAACGGTCTGGTC-3′, rv 5′-TATTCGCTGGTCACTTCGAT-3) and reference gene *Eef2* (fw 5′-AGGCCTGTGTAATATAGCTGCG-3′, rv 5′-CTCTGTGTAGTTTG-TAGCTCTGTCT-3′) (for details see [25]).

Genotyping of *Peds1*-deficient mice was performed by conventional PCR as recommended by the supplier, with Taq DNA polymerase (Thermo Fisher Scientific, Waltham, MA, USA) and primers for the transgenic allele (fw 5′-GCGTGTCCTGCTGAGACTTG-3′ and rv 5′-TCGTGGTATCGTTATGCGCC-3′) and primers for the wildtype allele (fw 5′-GCGTGTCCTGCTGAGACTTG-3′ and rv 5′-CATCCCACCTATCC-CACCTG-3′).

2.3. Mouse tissues for lipidomic analysis and Western blot

For tissue harvest, 8-week-old male homozygous knockout mice and their sex-matched wildtype littermates were sacrificed by cervical dislocation. We restricted the analysis to one sex due to the cost- and time-intensive lipidomics measurement and data analysis. Tissues were extracted, snap frozen in liquid nitrogen, stored at −80 °C and shipped on dry ice for further analysis. For lipidomic analysis, following tissues were extracted (five biological replicates per group): cerebrum, cerebellum, liver, sWAT and vWAT for *Agmo*-deficient mice and cerebrum, cerebellum, kidney, sWAT and vWAT for *Peds1*-deficient mice. For Western blot analysis cerebrum of *Peds1* knockout mice and wildtype controls were analyzed.

2.4. Lipidomic analysis

Lipidomic analysis of samples was performed at the Core Facility Metabolomics of the Amsterdam UMC, location AMC, Amsterdam, the Netherlands and was performed essentially as previously [34]. Internal standards and used amounts can be found in the supplemental methods. After the addition of the internal standards, 1.5 ml 1:1 (*v/v*) methanol:chloroform was added before thorough mixing. The samples were then centrifuged for 10 min at 14.000 rpm, supernatant transferred to a glass vial and evaporated under a stream of nitrogen at 60 °C. The residue was dissolved in 150 µl of 1:1 (*v/v*) methanol:chloroform. Lipids were analyzed using a Thermo Scientific Ultimate 3000 binary HPLC coupled to a Q Exactive Plus Orbitrap mass spectrometer. For normal phase separation, 5 µl of each sample was injected onto a Phenomenex® LUNA silica, 250 * 2 mm, 5 µm 100 Å. Column temperature was held at 25 °C. Mobile phase consisted of (A) 85:15 (*v/v*) methanol:water containing 0.0125 % formic acid and 3.35 mmol/l ammonia and (B) 97:3 (*v/v*) chloroform:methanol containing 0.0125 % formic acid. Using a flow rate of 0.3 ml/min, the LC gradient consisted of: isocratic at 10 % A 0–1 min, ramp to 20 % A at 4 min, ramp to 85 % A at 12 min, ramp to 100 % A at 12.1 min, isocratic at 100 % A 12.1–14 min, ramp to 10 % A at 14.1 min, isocratic at 10 % A for 14.1–15 min. For reversed phase separation, 5 µl of each sample was injected onto a Waters HSS T3 column (150 × 2.1 mm, 1.8 µm particle size). Column temperature was held at 60 °C. Mobile phase consisted of (A) 4:6 (v/v) methanol:water and (B) 1:9 (v/v) methanol:isopropanol, both containing 0.1 % formic acid and 10 mmol/l ammonia. Using a flow rate of 0.4 ml/min, the LC gradient consisted of: isocratic at 100 % A at 0 min, ramp to 80 % A at 1 min, ramp to 0 % A at 16 min, isocratic at 0 % A for 16–20 min, ramp to 100 % A at 20.1 min, isocratic at 100 % A for 20.1–21 min. MS data were acquired using negative and positive ionization by continuous scanning over the range of *m/z* 150 to m/z 2000 at a resolution of 280,000 full width at half maximum height. Data were analyzed using an in-house developed lipidomics pipeline written in the R programming language (http://ww.r-project.org) and MATLAB. Lipid identification was based on a combination of accurate mass, (relative) retention times, fragmentation spectra (when required), analysis of samples with known metabolic defects, and the injection of relevant standards. Lipid classes are defined in our lipidomics pipeline in terms of their generic chemical formula, where R represents the radyl group. Upon import of the lipid database in the annotation pipeline the generic chemical formula of each lipid class is expanded by replacing the R-element with a range of possible radyl group lengths and double bond numbers. The resulting expanded list of chemical formulas is then used to calculate the neutral monoisotopic mass of each species. The reported lipid abundances are semi-quantitative and calculated by dividing the response of the analyte (area of the peak) by that of the corresponding internal standard multiplied by the concentration of that internal standard (arbitrary unit, A.U). In the case where no appropriate internal standard was present for a certain class of lipids, their intensities were normalized on the intensity of one internal standard (usually PE[28:0]), to correct for inter-batch variation only. From these, only MG and its corresponding ether species were included in the results. The PC[O] and PE[O] species elute later on the reversed phase column than the corresponding PC[P] and PE[P] species as can be seen in supplemental Fig. S1 which depicts the data analyzed in this study. The WT/PEDS1 comparison where no [P] species are annotated and [O] species accumulate confirms the correct annotation of the isobaric ether lipid species. When the exact ether lipid side chain was unknown or could not be separated chromatographically, the sum of alkyl and alkenyl ether lipid species (indicated as [O + P]) obtained from the normal phase column analysis were used as seen in TG [O + P], LPA[O + P] and PA[O + P]. Based on the assumption that same class lipids responded equally as their respective internal standard, only relative abundances within the same species can be used to calculate total lipid levels and compared between different sample groups (e.g. knockout versus wildtype). Relative concentrations between different species are not directly comparable.

2.5. Immunoblot analysis

Cerebral cortex homogenates of *Peds1*-deficient mice and wildtype controls were prepared in five volumes ice-cold homogenizing buffer containing 0.25 M sucrose, 20 mM HEPES-KOH, pH 7.4, 1 mM EDTA, 1 mM PMSF, and cOmplete™ protease inhibitor cocktail (Sigma, Tokyo,

Japan) and the protein concentration was determined using Pierce BCA protein assay reagent (Thermo Fisher Scientific, Tokyo, Japan). Eight micrograms of protein were analyzed by sodium dodecyl sulfate-polyacrylamide gel electrophoresis (SDS-PAGE) and immunoblotting with rabbit polyclonal antibody to FAR1 [7].

2.6. Data presentation and statistics

Statistics of lipidomic analysis was done per lipid class if a sufficient number of metabolites was available (greater than the sample number to prevent overfitting of the data). Statistical analysis could not be performed when lipid species contained too many missing values. Results obtained from immunoblotting experiments were analyzed by one-tailed Student's *t*-test. Results were visualized with R and GraphPad Prism 9.0.1.

3. Results

3.1. Changes in lipid species upon Peds1 knockout

We analyzed the overall lipidomic changes in tissues of *Peds1* knockout mice as well as their respective wildtype controls in five biological replicates per group by high-resolution mass spectrometry. Up to 1875 lipid species, depending on the analyzed tissue, were identified which fulfilled initial quality criteria (see lipidomic data analysis in Material and Methods). In order to understand the impact of the knockout on the tissue lipidome, we compared the relative abundances of lipid species with those found in their wildtype controls in the following selected tissues: two brain regions, cerebrum and cerebellum, subcutaneous and visceral white adipose tissue (sWAT and vWAT, respectively) and kidney for *Peds1*.

As ether lipids and plasmalogens, the PEDS1 products, are especially abundant in the brain [35], we first analyzed the impact of *Peds1* knockout on lipid species in this lipid rich tissue. In total, we identified 372 changed lipid species in cerebrum (247 elevated, 125 reduced, cut off: $P = 0.01$, fold change = 2; Fig. 1A, left panel) and 374 changed lipid species in cerebellum (243 accumulated, 131 depleted species, cut off: P = 0.01, fold change = 2; supplemental Fig. S2A, left panel). Both brain regions displayed noticeable changes upon *Peds1* deficiency characterized by a strong accumulation of plasmanyl lipid species [O] and a striking reduction in the vast majority of plasmenyl lipid species [P]. These changes were not only found in ether glycerophospholipids including lyso-phospatidylcholines (LPC[O/P]), lyso-phosphatidylethanolamines (LPE[O/P]), phosphatidylcholines (PC[O/P]) and phosphatidylethanolamines (PE[O/P]) but were also mimicked by neutral glycerolipids like plasmanyl/plasmenyl monoacylglycerols (MG[O/P]) and plasmanyl/plasmenyl diacylglycerols (DG[O/P]). These profound changes were also detected in ether lipid classes where the nature of the ether-bond at the *sn*-1 position could not be separated into plasmanyl and plasmenyl species (see lipidomic data analysis in Materials and Methods for details) i.e. lyso-phosphatidic acids (LPA[O + P]), phosphatidic acids (PA[O + P]) and triacylglycerols (TG[O + P]) (represented as diamonds). For LPA[O + P] and PA[O + P], individual lipid species were found to be either clearly elevated or reduced mimicking the behavior of alkyl versus alkenyl species seen in lipid classes where resolution of these two subclasses was feasible. The subclass of TG[O + P] was overall strongly accumulated indicating that this class was clearly consisting of mostly plasmanyl species.

The influence of *Peds1* knockout on other lipid classes, beyond those discussed above, was less incisive with only individual lipid species being increased e.g. in the class of bis(monoacylglycero)phosphate (BMP; in cerebrum one of 35 detected BMP lipid species; in cerebellum three of 38 detected BMP lipid species, cut off: $P = 0.01$, fold change = 2) or decreased e.g. in the class of hexosylceramide (HexCer[d]; three of 42 detected HexCer[d] species in cerebrum, one of 45 detected HexCer [d] lipid species in cerebellum, cut off: P = 0.01, fold change = 2).

Next, we focused on lipidomic alterations in the kidney (Fig. 1B, left panel) of *Peds1*-deficient mice as it is the tissue with the highest PEDS1 activity [35]. In the 163 significantly changed lipid species resulting from 69 increased and 94 decreased species (cut off: P = 0.01, fold change = 2) in kidney, we identified an accumulation of plasmanyl lipid species concomitant with a reduction of plasmenyl lipid species although this effect was weaker than in both analyzed brain regions. In kidney, changes were restricted to PC[O], PC[P], PE[O], PE[P] and their respective lyso-forms while minor changes could be observed in DG[O] and DG[P]. Again, changes in single lipid species of diverse ester lipids (cholesteryl ester, CE; dihexosylceramide, Hex2Cer; phosphatidylglycerol, PG) were found whereby the most striking changes were detected in the PE class where a significant decrease of 12 individual lipid species and an increase of 1 lipid species from a total of 64 detected lipid species was found (cut off: $P = 0.01$, fold change = 2, Fig. 1B, left panel; supplemental Fig. S3). No preferences for carbon chain length nor the degree of saturation was observed in these changed PE lipid species.

As prominent effects were found in the lipid-rich tissue brain, we then also looked into the lipid composition of the two different fat tissues, sWAT (Fig. 1C, left panel) and vWAT (supplemental Fig. S2B, left panel). In sWAT, from 56 significantly changed lipid species, 40 were increased while 16 were reduced (cut off: $P = 0.01$, fold change = 2). We detected an enrichment of plasmanyl lipid species and a reduction of plasmenyl lipid species in all ether glycerophospholipid subclasses. However, neutral glycerolipids MG[O] and MG[P] were not changed and DG[O] and DG[P] lipid species could not be assessed as their signal was masked by the massive amounts of DG present in fat tissues. In sWAT, single lipid species of TG[O + P] were significantly decreased while in vWAT TG[O + P] showed an overall reduction. There, 11 significantly changed species were detected of which 6 were accumulated and 5 were depleted (cut off: $P = 0.01$, fold change = 2). However, the changes in vWAT were generally less significant than in sWAT.

Boxplots showing nine glycerolipid classes divided in ether and ester species for *Peds1* knockout and wildtype controls can be found in supplemental Figs. S4 (kidney), S5 (cerebrum and cerebellum) and S6 (sWAT and vWAT). Detailed information on the relative abundance of each lipid species of PE, PC, LPE, LPC, MG, DG and TG lipid classes can be found in supplemental Figs. S7–13 for kidney, S14–20 for cerebrum, S21–27 for cerebellum, S28–33 for sWAT and S34–39 for vWAT.

Altogether, the effects of *Peds1* knockout on the lipid composition were pronounced and consisted of reduced plasmenyl species and concomitantly increased plasmanyl lipids. Changes were mainly restricted to the subclasses of ether lipids with a certain variation depending on the analyzed tissue.

3.2. Changes in lipid species upon Agmo knockout

To characterize changes upon *Agmo* deficiency, tissues were selected according to the same criteria as for *Peds1* knockout i.e. cerebrum, cerebellum, sWAT, vWAT and the tissue with the highest AGMO activity, the liver [13]. Overall, changes in *Agmo* knockout mice were much less pronounced as compared to *Peds1* knockout mice (3–64 significantly changed lipid species in *Agmo* knockout versus 11–374 significantly changed lipid species in *Peds1* knockout) and were primarily marked by accumulation of all ether lipid species (plasmanyl and plasmenyl lipid classes likewise) whereas ester lipid levels were maintained at wildtype levels. In cerebrum, we found six significantly elevated lipid species (cut off: $P = 0.01$, fold change = 2; Fig. 1A, right panel) which included three species of LPC[P] (LPC[P-18:0], LPC[P-20:0], LPC[P-20:1]) and one species each of LPC[O], PC[O] and MG[O] (LPC[O-17:0], PC[O-34:4], MG[O-16:1]). In cerebellum, only three significantly increased lipid species were detected (cut off: P = 0.01, fold change = 2; supplemental Fig. S2A, right panel) which had already been found also in cerebrum (LPC[P-20:0], LPC[O-17:0], PC[O-34:4]). More prominent changes were detected in the liver where 59 lipid species were significantly accumulated (cut off: P = 0.01, fold change = 2; Fig. 1B, right panel).

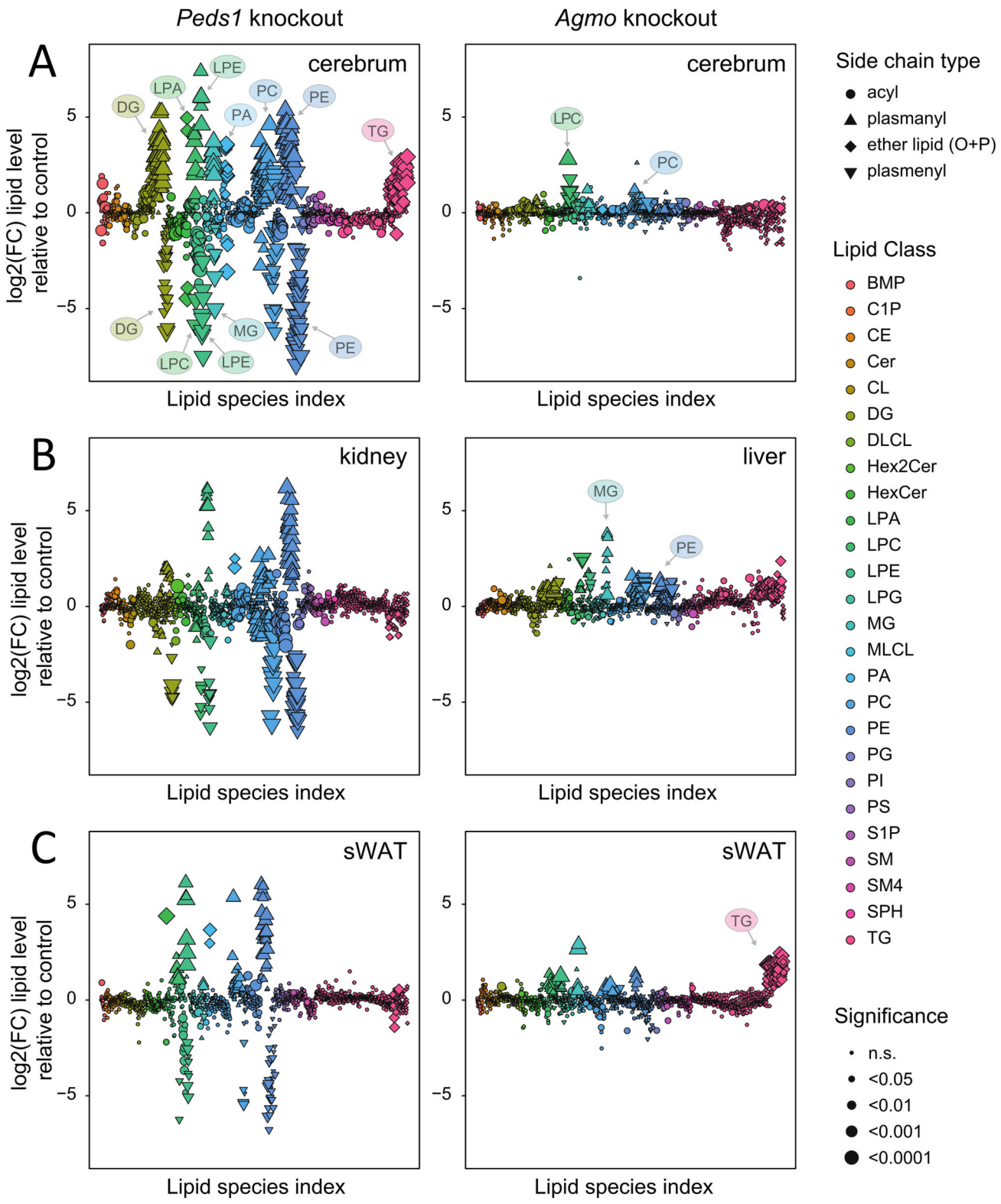

Fig. 1. Changes of single lipid species upon *Peds1* (left panels) or *Agmo* (right panels) knockout A) in the ether lipid-rich tissue cerebrum, B) in the tissue with highest enzymatic activity, i.e. kidney for *Peds1* knockout (left) and liver for *Agmo* knockout (right) and C) in the lipid-rich tissue sWAT. Knockout mice were compared to wildtype controls and calculated fold changes (y-axis, as log2) as well as *p*-values (symbol size) are illustrated. sn-1 bondage is distinguished by circles (acyl), upward-pointing triangles (plasmanyl), downward-pointing triangles (plasmenyl) and diamonds (unresolved plasmanyl and plasmenyl lipids). C1P[d]: ceramide-1-phosphate, Cer[d]: ceramide, CE: cholesteryl ester, Hex2Cer[d]: dihexosylceramide, Hex2Cer[t]: hydroxy-dihexosylceramide, HexCer[d]: hexosylceramide, HexCer [t]: hydroxyhexosylceramide, LPG: lysophosphatidylglycerol, MLCL: monolysocardiolipin, PG: phosphatidylglycerol, PI: phosphatidylinositol, S1P: sphinganine-1-phosphate, SM[d]: sphingomyelin, SM[t]: hydroxysphingomyelin, SM4[d]: sulfatide, SM4[t]: hydroxysulfatide, SPH[d]: sphinganine.

Here, individual species of glycerophospholipids PC[O], PC[P], PE[O], PE[P] and their lyso-forms as well as neutral glycerolipids MG[O], DG [O], DG[P] and TG[O + P] were enhanced. Finally, in sWAT, 64 significantly increased lipid species were found (cut off: P = 0.01, fold change = 2; Fig. 1C, right panel) while in vWAT 54 significantly accumulated lipid species and two significantly reduced lipid species were detected (cut off: P = 0.01, fold change = 2; supplemental Fig. S2B, right panel). These species belonged to the subclasses of LPC[O], LPE[O], PC

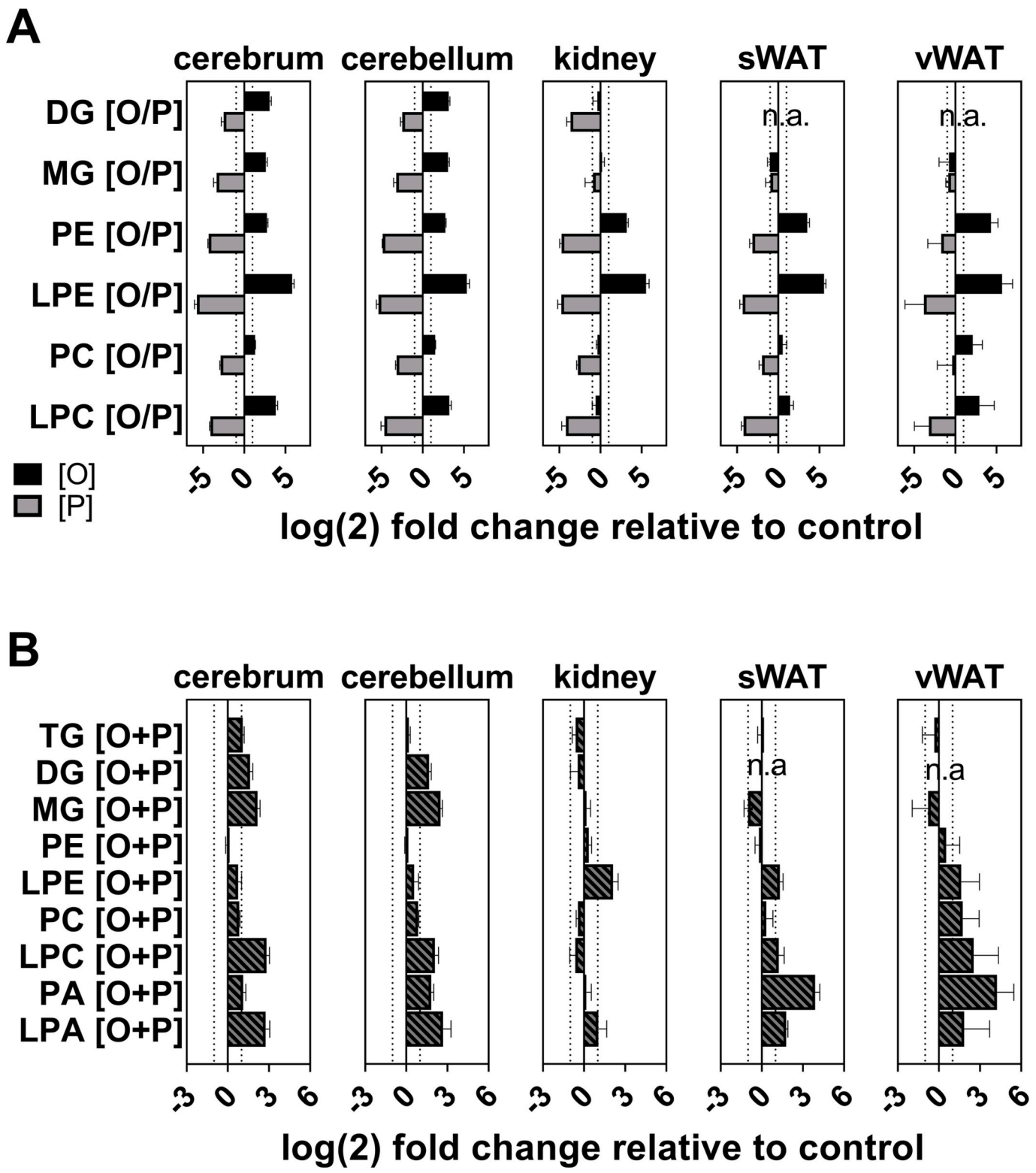

Fig. 2. Impact of *Peds1* knockout on ether lipid levels in five selected tissues. A) Changes of plasmanyl ([O], in black) and plasmenyl ([P], in gray) lipid classes. B) Bar charts showing the fold changes of summed total ether lipids ([O + P], black/gray patterned) in *Peds1*-deficient tissues relative to the wildtype control. Relative abundances of lipid subclasses were compared to wildtype control for calculating the fold change (as log(2)) in cerebrum, cerebellum, kidney, sWAT and vWAT. Dashed line at −1 and 1 indicates a fold change of 2. n.a. = data not available. Data is presented as mean ± SD ($n = 5$).

[O] as well as PE[O] with the most fundamental effects seen in the neutral glycerolipids MG[O] and TG[O + P]. Again, DG[O] and DG[P] lipid species could not be analyzed in the fat tissue of *Agmo* knockout mice as observed also in *Peds1* mice. Supplemental Fig. S40 (liver), Fig. S41 (cerebrum and cerebellum) and Fig. S42 (sWAT and vWAT) show boxplots of seven glycerolipid classes divided in ether and ester species for *Agmo* knockout and wildtype controls. Bar charts showing the abundance of each lipid species of PE, PC, LPE, LPC, MG, DG and TG lipid classes can be found in supplemental Figs. S43–49 for liver, S50–56 for cerebrum, S57–63 for cerebellum, S64–69 for sWAT and S70–75 for vWAT. In all analyzed tissues, beyond the ether lipids already mentioned, no prominent changes in the lipid species of other lipid classes were detected.

In contrast to the *Peds1* knockout, in the *Agmo* knockout less pronounced changes were found. *Agmo* deficiency was characterized by an increase of most ether lipid classes irrespective of presence of the vinyl ether double bond.

3.3. Impact of Peds1 deficiency on ether lipids

To better understand the regulation of ether lipids in the absence of PEDS1, we investigated the balance between plasmanyl and plasmenyl ether lipids and which ether lipid subclasses presented the most striking changes.

Highest accumulations of plasmanyl lipids (Fig. 2A, black bars) were detected in LPE[O] for all tested tissues ranging from 42.1 to 68.8 fold while the respective plasmenyl lipids (Fig. 2A, gray bars) decreased in a range from 20.6 to 55.2 fold with the lowest alterations in vWAT. This characteristic accumulation of plasmanyl lipids and a reduction in plasmenyl lipids was also found in diverse ether lipid subclasses of all tested tissues, while both brain regions showed this effect in all analyzed ether lipid subclasses. Strikingly, kidney presented nearly unchanged levels in LPC[O] (1.47 fold decreased), PC[O] (1.29 fold decreased) and DG[O] (1.24 fold decreased) while the respective plasmenyl lipids were presented with a prominent decrease (LPC[P]: 17.8 fold, PC[P]: 6.7 fold and DG[P]: 12.1 fold). Furthermore, no alterations in MG[O/P] (above the threshold of 2 fold) were found in kidney (MG[O]: 1.15 fold increased, MG[P]: 1.57 fold decreased), in vWAT (MG[O]: 1.35 fold decreased, MG[P]: 1.78 fold decreased). and in sWAT (MG[O]: 2.0 fold decreased, MG[P]: 1.8 fold decreased). In sWAT, PC[O] levels were unchanged (1.54 fold increased) although the respective plasmenyl counterpart was decreased (3.9 fold). In contrast, in vWAT no decrease in PC[P] was observed (1.3 fold decreased) while PC[O] presented the expected accumulation (2.51 fold increased).

Furthermore, we also examined whether total ether lipids (as the sum of [O + P]) were affected by the disbalance that occurs when plasmenyl lipids are missing. Fig. 2B shows that most ether lipid subclasses were elevated in *Peds1* knockout mice when compared to control. Strikingly, in all analyzed tissues, the sum of PE[O] plus PE[P], the most abundant ether lipid metabolites in the tissues was, however, not altered (ranging from 0.9 fold decreased in sWAT to 1.7 fold increased in vWAT). Thus PE[O] in *Peds1* knockout mice accumulates exactly to the same concentrations as PE[P] were present in the wildtypes. In kidney, the organ with highest PEDS1 activity [35], the sum of the other ether lipid classes, which quantitatively are of minor importance as compared to the PE[P]s and PE[O]s, remained largely unchanged upon *Peds1* knockout (Fig. 2B).

3.4. Impact of Agmo deficiency on AGMO substrates

When looking at the AGMO lipid substrates [36], i.e. lysoalkylglycerophospholipids (LPC[O] and LPE[O], Fig. 3 left panels) and alkylglycerols (MG[O], Fig. 3 right panels), necessarily carrying a hydroxyl group at the sn-2 position, we detected a significant accumulation of 25 individual lipid species. Within these lipids, 14 carried a completely saturated alkyl side chain at *sn*-1, further nine species were monounsaturated and two lipid species harbored two double bonds in their side chain. The latter two were MG[O-20:2] in liver (Fig. 3A, right panel) and MG[O-18:2] in sWAT (Fig. 3D, right panel). Twenty of these 25 species had side chains with ≥18 carbon atoms while the remaining five species carried side chains with 14–17 carbon atoms and were selectively present in both brain regions and in sWAT (i.e. LPC[O-17:0] in cerebrum and cerebellum (Fig. 3B + C, left panel), MG[O-16:1] in cerebrum (Fig. 3B, right panel) and LPC[O-14:0], LPC[O-16:0] and LPC [16:1] in sWAT (Fig. 3D, left panel). Interestingly, MG[O-20:0] and MG [O-22:1] were elevated in all tested tissues except for brain. Overall, these data may indicate that AGMO preferably accepts completely saturated or monounsatured lipid species with ≥18 carbon atoms.

3.5. FAR1 protein amount in cerebral cortex in Peds1 deficiency

As FAR1 is the rate-limiting enzyme in peroxisomal ether lipid biosynthesis and it is proposed to sense high levels of plasmalogens which leads to its degradation, we evaluated FAR1 protein expression in cerebral cortex of *Peds1*-deficient mice, in which plasmalogens are depleted while plasmanyl lipids are increased. Consistent with the unchanged amount of PE[O + P], *Peds1* knockout mice showed no significant differences in FAR1 protein expression when compared to wildtype controls (Fig. 4). Thus, we can conclude that loss of plasmenyl lipids is not enough to raise FAR1 levels. Whether FAR1 activity is also affected by the observed changes in plasmanyl and plasmenyl lipids remains to be investigated.

4. Discussion

The aim of this study was to investigate the molecular changes of the global lipid pool occurring when two ether lipid metabolizing enzymes, i.e. AGMO of the catabolic route and PEDS1 of the anabolic route, are knocked out in mice and whether these changes correlate with the impact on physiology observed in the knockout mice. We found that *Agmo* knockout triggered only mild changes in the lipidome seen as modest increases only in plasmanyl and plasmenyl lipids. On the other hand, *Peds1* knockout manifested profound alterations of the lipid profile which was hallmarked by complete absence of plasmalogens paralleled by accumulation of plasmanyl lipids. Both of the assigned metabolic changes are in good accordance with the severity of the phenotypes identified in *Agmo*- and *Peds1*-deficient mice, reflected by absence of a specific *Agmo*-deficient phenotype whereas *Peds1* knockout manifests a phenotype mostly affecting growth and blood parameters.

In the *Agmo* knockout mice the most significant changes in the lipidome were found in the liver, which is the organ where AGMO is most abundantly expressed and active [13]. Plasmalogen levels are known to be very low in mouse wildtype liver [14], a finding we could confirm and extend to all ether lipid species present in our dataset. We found an overall moderate elevation of both plasmanyl and plasmenyl lipid species in all ether lipid subclasses in *Agmo*-deficient liver while in the other analyzed tissues only certain ether lipid subclasses were significantly affected (see right panels of Fig. 1 and supplemental Fig. S2). In sWAT and vWAT neutral ether lipids (i.e. TG[O + P]) were accumulated.

Both brain regions, cerebrum and cerebellum, showed significantly higher levels of LPC[O], LPC[P] and PC[O] but the highly abundant PE [O/P] were not influenced by the *Agmo* knockout. To better understand and summarize the consequences of *Agmo* knockout on the ether lipid metabolism in the different tissue types analyzed in our study, we highlighted the changes of ether lipid subclasses compared to wildtype controls (see metabolic scheme of ether lipids in Fig. 5). Moderate accumulation of AGMO substrates MG[O] and LPC[O] as well as LPC[P] were found in cerebrum (Fig. 5B right panel). *Agmo* knockout in sWAT was characterized with enhanced levels of solely AGMO substrates LPC [O], LPE[O] and MG[O] (Fig. 5D right panel). However, the most pronounced but still mild changes were detected in the liver seen as enhanced levels of all plasmanyl and plasmenyl lipid subclasses

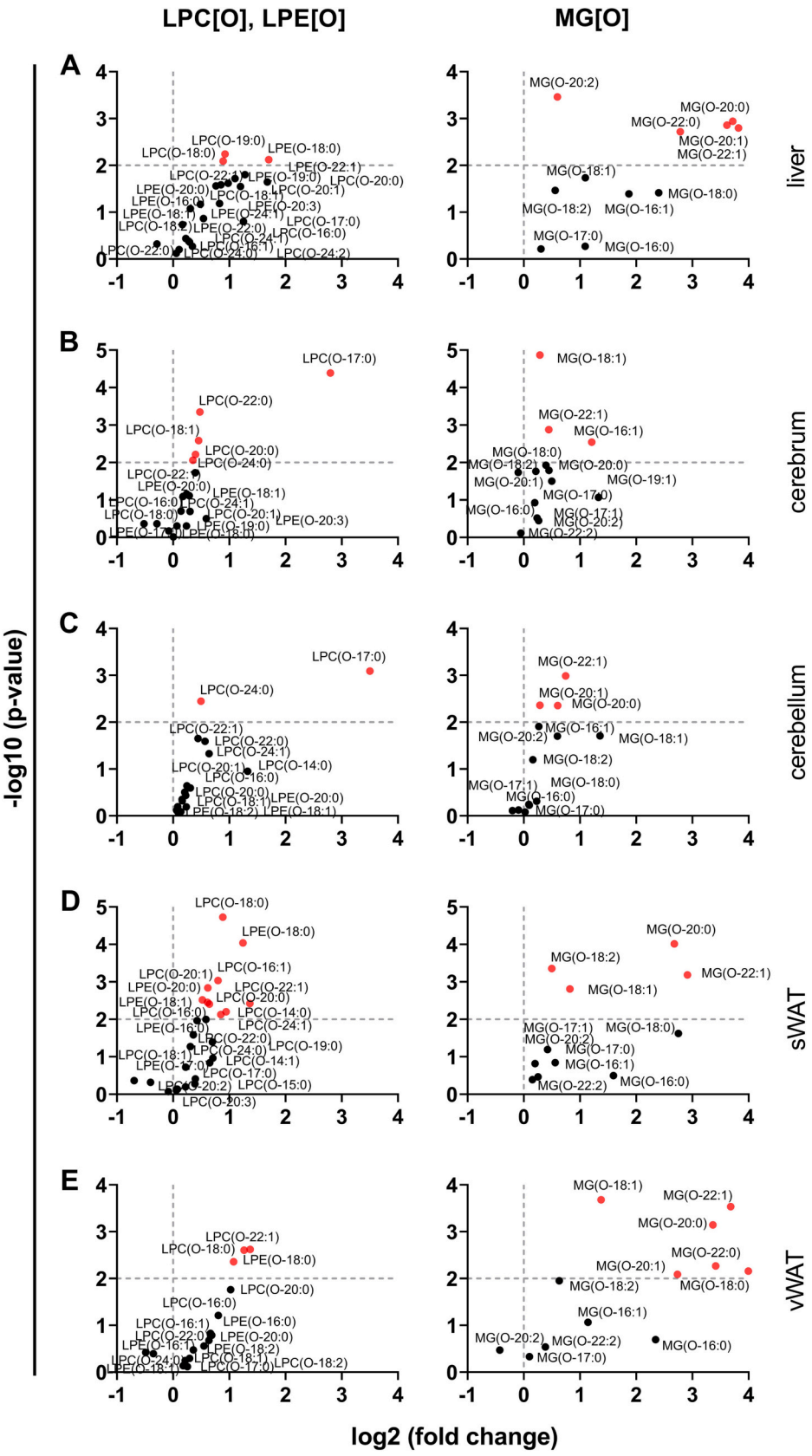

Fig. 3. Volcano plot highlighting changes in Agmo substrates in all tested tissues. Lysoalkylglycerophospholipids (LPC[O], LPE[O], left panel) and alkylglycerol (MG[O], right panel) changed in *Agmo* knockout mice compared to wildtype mice in A) liver, B) cerebrum, C) cerebellum, D) sWAT and E) vWAT. The significance cut-off ($P < 0.01$) is indicated as horizontal dashed line. The vertical dashed line separates log2 (fold change) of decreased and increased (red dots) lipid species (n = 5). (For interpretation of the references to colour in this figure legend, the reader is referred to the web version of this article.)

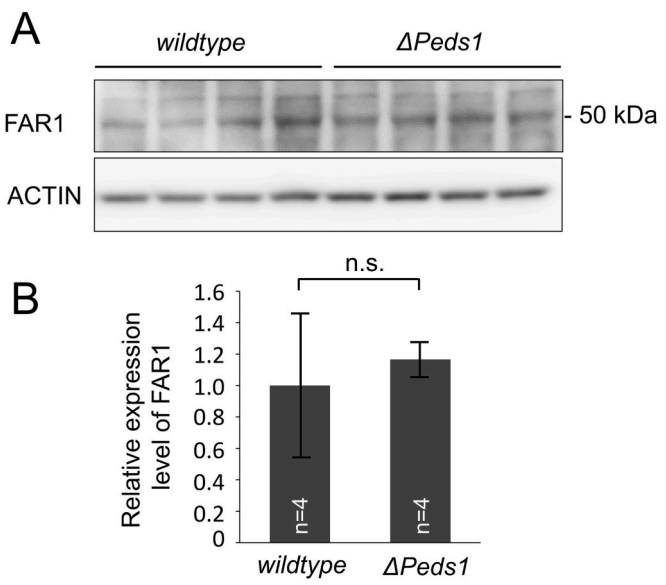

Fig. 4. Effect of Peds1 deficiency on the amount of FAR1 protein expression in cerebral cortex. A) Representative immunoblot analysis of FAR1 in the cerebral cortex of *Peds1* knockout mice (ΔPeds1) and wildtype controls is shown. ACTIN was used as loading control. B). Relative expression level of FAR1 in *Peds1* knockout mice was represented by taking expression levels in wildtype as one. $n = 4$, data shown as mean ± SD. n.s. = not significant.

(including the substrates of AGMO) except for PC[O], PE[O] and PE[P] (Fig. 5C right panel). These quite mild changes we observed in all tissues mirror the fact that *Agmo*-deficient mice do not display a phenotype under standard housing conditions present in the SPF facility. In a setting where the AGMO pathway is not stimulated, accumulating plasmanyl lipids can be cleared via the plasmalogen branch of ether lipid metabolism where the respective lysoplasmalogenase degrades excessive amounts independently of the AGMO enzyme [37]. In a former study in the murine RAW264.7 macrophage cell line, where we applied lentiviral knockdown of *Agmo*, we found significantly altered levels of glycosylated ceramides and cardiolipins [18]. This was not observed in our current lipidome of *Agmo* knockout tissues. As we had to rely on cluster analysis and lipid subclass enrichment as strategies to attribute peaks to certain lipid species for the RAW264.7 study despite the use of high-resolution mass spectrometry, our current study is much more accurate as it benefits from the many advances that have been made in this field in the meantime ([33], for review see [38]). Also for the class of sphingolipids we did not observe prominent changes. This was surprising as previous findings in human cells had found a dependency and co-regulation of ether lipids and ceramides [39] as well as increased SM levels in *Gnpat* knockout mice, which lack all ether lipids [40]. From this perspective the general absence of all ether lipids by disruption of early synthetic pathways has a more profound impact on lipids even outside the ether lipid pool. Such an alteration has more impact than switching off a single catabolic route in this pathway for which a salvage route via plasmalogen synthesis and degradation plausibly exists.

In the *Peds1* knockout mouse model we found marked changes in the lipidome of all five analyzed tissues. Metabolic changes of ether lipid subclasses in the different tissues (highlighted in the metabolic scheme Fig. 5 B-D, left panels) presented a dramatic decrease in all analyzed plasmalogen subclasses of cerebrum, kidney and sWAT. In the brain, this was accompanied by a dramatic increase of all analyzed plasmanyl species highest in LPE[O] followed by LPC[O], DG[O] and PE[O] (Fig. 5B left panel). Similar but weaker accumulations were also detected in sWAT (Fig. 5D, left panel) while in kidney (Fig. 5C, left panel) only PE[O] and LPE[O] subclasses were enriched. Nevertheless, this points to a strong feedback from PE[O] to LPE[O] and additionally DG[O] from which further accumulation of other plasmanyl subclasses can occur, when PEDS1 is absent. Furthermore, kidney presented with a slight reduction in PC[O] in *Peds1*-deficient mice, a finding which is in contrast to the general trend of PC[O] accumulation found in the other tested tissues. This contradiction was also found in a previous study, where we had analyzed PC[O/P] and PE[O/P] species in *Peds1*-deficient mouse kidneys [33].

In our lipidomic analysis, we found in kidney that the observed changes of PE[O/P] subclasses had a minor impact on the ester PE subclass for which 12 out of 64 detected species were decreased (cut off: $P = 0.01$, fold change = 2, supplemental Fig. S3). This principle of a cellular phospholipid homeostasis, i.e. that the sum of the total cellular phospholipid species of a lipid subclass is kept constant, was already described for PE lipids in fibroblasts of rhizomelic chondrodysplasia punctata patients as well as in brains of *Gnpat*-deficient mice, which are not able to synthesize any ether lipids [40].

FAR1 was identified as a key regulatory point in ether lipid biosynthesis with FAR1 protein found to be upregulated in human cells [7] or mouse cerebellum [41] defective in GNPAT activity which lack both, PE[O] and PE[P]. Additionally, the protein levels of FAR1 could be normalized by adding PE[P] but not PE to the cells [7]. Whether also PE[O]s address this feedback inhibition mechanism has so far been unknown. Here, we find that the amount of PE[O] accumulated in tissues of *Peds1*-deficient mice accurately resembles the amount of PE[P] in the corresponding wildtype tissues. In cerebrum, the tissue with the highest PE[P] levels, we found that the amount of FAR1 protein remained unchanged upon the *Peds1* knockout (Fig. 4). This suggests that both PE[O] and PE[P] may lead to feedback inhibition on FAR1 (Fig. 6).

Detailed lipidomic studies of ether lipids are rarely found as the appropriate technologies are just emerging. Compared to our study, others recently reported the presence of ether-linked glycerophospholipids in several murine tissues and brain regions as well but did not provide a clear separation between alkyl- and alkenyl-linked phospholipids [42,43]. In our high resolution MS analysis we were able to discriminate between plasmanyl and plasmenyl lipid subclasses not only in phospholipids but also for neutral lipids. So far, in literature, only few lipidomic data is available on monoalkyl-diacylglycerols (i.e. TG[O]) from murine tissues [44]. As the analytical tools for the analysis of neutral ether lipids have also been meanwhile optimized, more reliable data like those in our present study are expected to soon become available.

In conclusion, we have found that the severity of the phenotypes of two mouse models deficient in one of the ether lipid metabolizing enzymes AGMO and PEDS1 are mirrored on the lipidomic levels. While profound changes are seen if PEDS1 is missing, surprisingly *Agmo* knockout has little impact on the mouse lipidome. This is possibly due to efficient feedback regulation of ether lipid biosynthesis and the possibility of alternative degradation routes after introduction of the vinyl ether double bond. An open question remains whether a strong accumulation of plasmanyl lipids would elicit physiological overall changes. Other issues that also need to be resolved in further studies is whether the reduced plasmalogen levels that have been implicated in neurodegenerative disorders like Alzheimer's or Parkinson's disease coincide with reduced or enhanced plasmanyl ether lipid species and whether these associations found are specific for plasmalogens or in general for all ether lipids [6].

Our analysis about the impact of AGMO and PEDS1 on the mouse lipidome takes us a step further in understanding the homeostasis of the lipid environment upon selective ether lipid deficiency in a living organism. This study also points to the importance of discriminating between plasmanyl lipids and plasmalogens in both neutral lipid and phospholipid classes, which is now possible by the proceedings in high-resolution analytics.

Supplementary data to this article can be found online at https://doi.org/10.1016/j.bbalip.2023.159285.

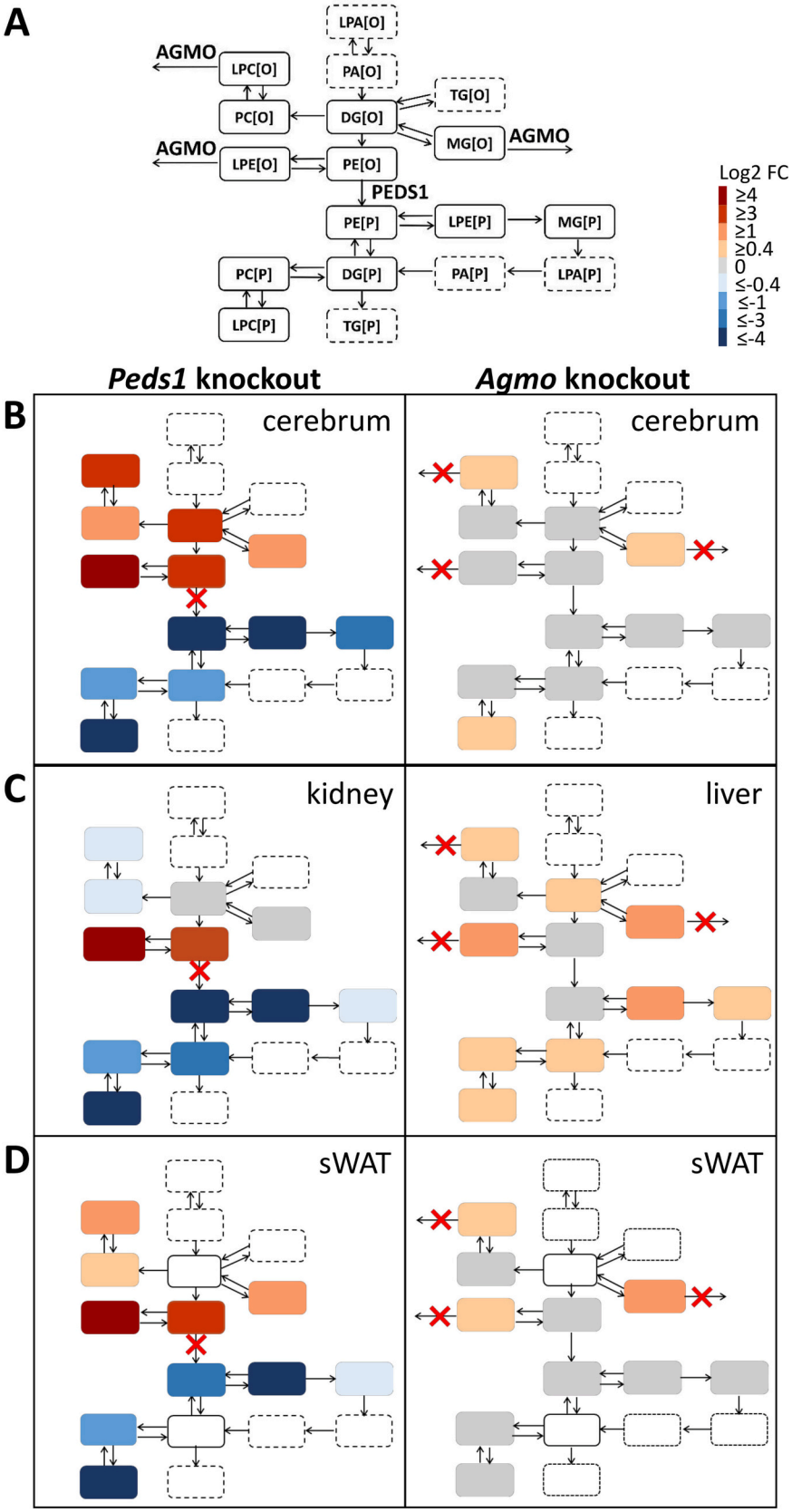

Fig. 5. Metabolic scheme of post-peroxisomal ether lipid metabolism in wildtype mice and changes in ether lipid metabolism upon either Peds1 or *Agmo* knockout. A) Schematic drawing of post-peroxisomal biosynthesis and remodeling in the ER which starts with LPA[O] that is converted to PA[O] and further metabolized to DG[O]. From DG[O] the metabolic scheme branches to TG[O], to the AGMO substrate MG[O], to PC[O] and to PE[O]. And from the latter two, the AGMO substrates LPC[O] and LPE [O] are then formed. PE[O] is used by PEDS1 to build PE [P] from which LPE[P] and DG[P] arise which can be further converted to MG[P], LPA[P], PA[P] as well as TG [P], PC[P] and LPC[P] in consecutive order. Alterations of ether lipid subclasses upon Peds1 (left panel) and Agmo (right panel) knockout B) in the ether lipid-rich tissue cerebellum, C) in tissues with highest enzymatic activity: kidney for *Peds1* knockout and liver for *Agmo* knockout and D) in the lipid-rich organ sWAT. The levels of each lipid subclass were compared to the wildtype control for calculating the fold change (as log2). Positive log2 fold changes were illustrated as a gradient from gray to dark red and the negative log2 fold changes from gray to dark blue. [O] = plasmanyl forms and [P] = plasmenyl forms of different lipid classes. Dashed rectangles represent ether lipids that cannot be separated into [O] and [P]. This biosynthetic pathway was adapted from Nagan and Zoeller [2] and Malheiro, da Silva and Brites [45] proposed as the most likely variant of ether glycerolipid synthesis pathway. (For interpretation of the references to colour in this figure legend, the reader is referred to the web version of this article.)

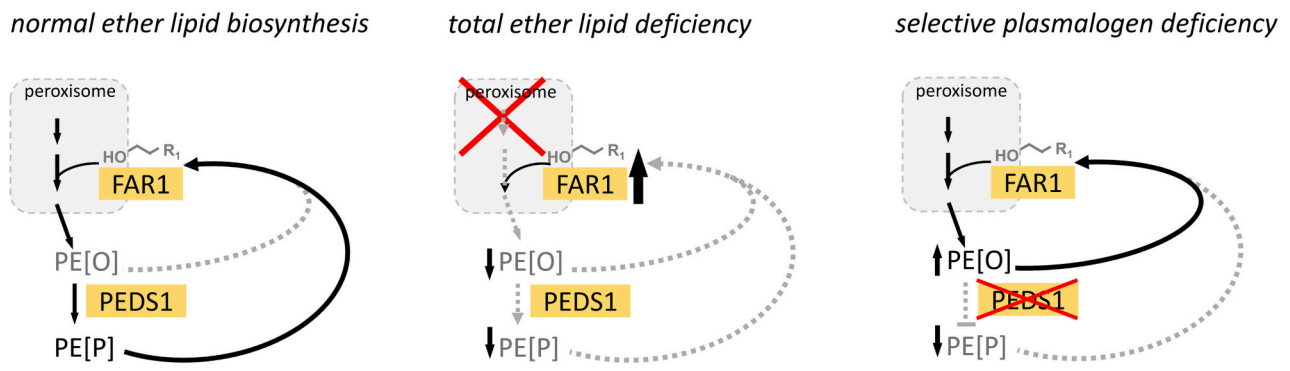

Fig. 6. Mechanism of FAR1 feedback regulation in intact and defective ether lipid metabolism. Left panel: In wildtype cells and tissues, ether-linked glycerophosphoethanolamines are almost exclusively present as PE[P] with PE[O] levels kept very low [33]. FAR1 senses these high levels of the end products PE[P] in a negative feedback mechanism where its protein levels are regulated accordingly to ensure stable ether lipid biosynthesis [7]. Central panel: Upon knockout of peroxisomal genes e.g. Gnpat (shown by the red cross), cells and tissues cannot produce PE[O/P]. As a compensatory mechanism, FAR1 protein levels are increased in order to fuel ether lipid biosynthesis [41]. Right panel: In contrast to a total ether lipid deficiency, the selective plasmalogen deficiency caused by knockout of Peds1 (indicated by the red cross), leads to FAR1 protein levels indistinguishable from wildtype. (For interpretation of the references to colour in this figure legend, the reader is referred to the web version of this article.)

Funding

This work was supported in part by the JSPS Grants-in Aid for Scientific Research Grant Nos. JP17K07337 and JP21K06839 (to MH), JP26116007, JP17H03675 (to YF); grants (to YF) from the Takeda Science Foundation and the Novartis Foundation (Japan) for the Promotion of Science and by the Austrian Science Fund (FWF) projects P30800 and P34723 (to K.W.).

CRediT authorship contribution statement

Katharina Lackner: Methodology, Software, Investigation, Writing – original draft. **Sabrina Sailer:** Methodology, Software, Investigation, Writing – original draft. **Jan-Bert van Klinken:** Formal analysis, Investigation, Data curation. **Eric Wever:** Formal analysis, Investigation, Data curation. **Mia L. Pras-Raves:** Formal analysis, Investigation, Data curation. **Adrie D. Dane:** Formal analysis, Investigation, Data curation. **Masanori Honsho:** Methodology, Investigation, Writing – original draft. **Yuichi Abe:** Methodology, Investigation. **Markus A. Keller:** Conceptualization, Supervision. **Georg Golderer:** Conceptualization, Supervision. **Gabriele Werner-Felmayer:** Conceptualization, Supervision. **Yukio Fujiki:** Writing – original draft, Supervision. **Frédéric M. Vaz:** Conceptualization, Supervision. **Ernst R. Werner:** Conceptualization, Writing – original draft, Supervision, Project administration. **Katrin Watschinger:** Conceptualization, Writing – original draft, Supervision, Project administration, Funding acquisition.

Declaration of competing interest

The authors declare that they have no known competing financial interests or personal relationships that could have appeared to influence the work reported in this paper.

Data availability statementRelative abundances of lipid subclasses and single lipid species can be found in supplemental data 1-4. The raw mass spectrometric data will be made available upon reasonable request (Institute of Biological Chemistry, Biocenter, Medical University of Innsbruck; katrin.watschinger@i-med.ac.at).

Relative abundances of lipid subclasses and single lipid species can be found in supplemental data 1-4. The raw mass spectrometric data will be made available upon reasonable request (Institute of Biological Chemistry, Biocenter, Medical University of Innsbruck; katrin.watschinger@i-med.ac.at).

Acknowledgements

We thank Petra Loitzl, Nina Madl, Nico Schöpf, Nadine Heinrich, Verena Scharf and Maria Fischer (all from the Medical University Innsbruck) for excellent technical assistance. The authors thank Jill Hermans and Martin Vervaart of the Core Facility Metabolomics of the Amsterdam UMC for the lipidomics analyses. We also thank the Wellcome Trust Sanger Institute Mouse Genetics Project (Sanger MPG) and its funders for providing the mutant mouse line *Tmem189*tm1a(KOMP) Wtsi and INFRAFRONTIER/EMMA (https://www.infrafrontier.eu/). Funding information may be found at https://www.sanger.ac.uk/science/collaboration/mouse-resource-portal and associated primary phenotypic information at https://www.mousephenotype.org/. The graphical abstract was created with BioRender.com.

References

[1] M. Oresic, V.A. Hänninen, A. Vidal-Puig, Lipidomics: a new window to biomedical frontiers, Trends Biotechnol. 26 (2008) 647–652, https://doi.org/10.1016/j.tibtech.2008.09.001.
[2] N. Nagan, R.A. Zoeller, Plasmalogens: biosynthesis and functions, Prog. Lipid Res. 40 (2001) 199–229, https://doi.org/10.1016/s0163-7827(01)00003-0.
[3] N.E. Braverman, A.B. Moser, Functions of plasmalogen lipids in health and disease, Biochim. Biophys. Acta (BBA) - Mol. Basis Dis. 1822 (2012) 1442–1452, https://doi.org/10.1016/j.bbadis.2012.05.008.
[4] C.D. Magnusson, G.G. Haraldsson, Ether lipids, Chem. Phys. Lipids 164 (2011) 315–340, https://doi.org/10.1016/j.chemphyslip.2011.04.010.
[5] N. Rangholia, T.M. Leisner, S.P. Holly, Bioactive ether lipids: primordial modulators of cellular signaling, Metabolites. 11 (2021), https://doi.org/10.3390/metabo11010041.
[6] F. Dorninger, S. Forss-Petter, I. Wimmer, J. Berger, Plasmalogens, platelet-activating factor and beyond - ether lipids in signaling and neurodegeneration, Neurobiol. Dis. 145 (2020), 105061, https://doi.org/10.1016/j.nbd.2020.105061.
[7] M. Honsho, S. Asaoku, Y. Fujiki, Posttranslational regulation of fatty acyl-CoA reductase 1, Far1, controls ether glycerophospholipid synthesis, J. Biol. Chem. 285 (2010) 8537–8542, https://doi.org/10.1074/jbc.M109.083311.
[8] S. Ferdinandusse, K. McWalter, H.Te Brinke, L. IJlst, P.M. Mooijer, J.P.N. Ruiter, A. E.M. van Lint, M. Pras-Raves, E. Wever, F. Millan, M.J.Guillen Sacoto, A. Begtrup, M. Tarnopolsky, L. Brady, R.L. Ladda, S.L. Sell, C.B. Nowak, J. Douglas, C. Tian, E. Ulm, S. Perlman, A.V. Drack, K. Chong, N. Martin, J. Brault, E. Brokamp, C. Toro, W.A. Gahl, E.F. Macnamara, L. Wolfe, Undiagnosed Diseases Network, Q. Waisfisz, P.J.G. Zwijnenburg, A. Ziegler, M. Barth, R. Smith, S. Ellingwood, D. Gaebler-Spira, S. Bakhtiari, M.C. Kruer, A.H.C. van Kampen, R.J.A. Wanders, H.R. Waterham, D. Cassiman, F.M. Vaz, An autosomal dominant neurological disorder caused by de novo variants in FAR1 resulting in uncontrolled synthesis of ether lipids, Genet. Med. 23 (2021) 740–750, https://doi.org/10.1038/s41436-020-01027-3.
[9] R. Liegel, B. Chang, R. Dubielzig, D.J. Sidjanin, Blind sterile 2 (bs2), a hypomorphic mutation in agps, results in cataracts and male sterility in mice, Mol. Genet. Metab. 103 (2011) 51–59, https://doi.org/10.1016/j.ymgme.2011.02.002.

[10] R. Liegel, A. Ronchetti, D. Sidjanin, Alkylglycerone phosphate synthase (AGPS) deficient mice: models for rhizomelic chondrodysplasia punctata type 3 (RCDP3) malformation syndrome, Mol. Genetics Metab. Reports 1 (2014) 299–311, https://doi.org/10.1016/j.ymgmr.2014.06.003.
[11] C. Rodemer, T.-P. Thai, B. Brugger, T. Kaercher, H. Werner, K.-A. Nave, F. Wieland, K. Gorgas, W.W. Just, Inactivation of ether lipid biosynthesis causes male infertility, defects in eye development and optic nerve hypoplasia in mice, Hum. Mol. Genet. 12 (2003) 1881–1895, https://doi.org/10.1093/hmg/ddg191.
[12] K. Gorgas, A. Teigler, D. Komljenovic, W.W. Just, The ether lipid-deficient mouse: tracking down plasmalogen functions, Biochim. Biophys. Acta 1763 (2006) 1511–1526, https://doi.org/10.1016/j.bbamcr.2006.08.038.
[13] K. Watschinger, M.A. Keller, G. Golderer, M. Hermann, M. Maglione, B. Sarg, H. H. Lindner, A. Hermetter, G. Werner-Felmayer, R. Konrat, N. Hulo, E.R. Werner, Identification of the gene encoding alkylglycerol monooxygenase defines a third class of tetrahydrobiopterin-dependent enzymes, Proc. Natl. Acad. Sci. U. S. A. 107 (2010) 13672–13677, https://doi.org/10.1073/pnas.1002404107.
[14] E.R. Werner, M.A. Keller, S. Sailer, K. Lackner, J. Koch, M. Hermann, S. Coassin, G. Golderer, G. Werner-Felmayer, R.A. Zoeller, N. Hulo, J. Berger, K. Watschinger, The TMEM 189 gene encodes plasmanylethanolamine desaturase which introduces the characteristic vinyl ether double bond into plasmalogens, Proc. Natl. Acad. Sci. U. S. A. 117 (2020) 7792–7798, https://doi.org/10.1073/pnas.1917461117.
[15] A. Tietz, M. Lindberg, E.P. Kennedy, A new pteridine-requiring enzyme system for the oxidation of glyceryl ethers, J. Biol. Chem. 239 (1964) 4081–4090. https://www.ncbi.nlm.nih.gov/pubmed/14247652.
[16] E.R. Werner, A. Hermetter, H. Prast, G. Golderer, G. Werner-Felmayer, Widespread occurrence of glyceryl ether monooxygenase activity in rat tissues detected by a novel assay, J. Lipid Res. 48 (2007) 1422–1427, https://doi.org/10.1194/jlr.D600042-JLR200.
[17] K. Watschinger, J.E. Fuchs, V. Yarov-Yarovoy, M.A. Keller, G. Golderer, A. Hermetter, G. Werner-Felmayer, N. Hulo, E.R. Werner, Catalytic residues and a predicted structure of tetrahydrobiopterin-dependent alkylglycerol monooxygenase, Biochem. J. 443 (2012) 279–286, https://doi.org/10.1042/BJ20111509.
[18] K. Watschinger, M.A. Keller, E. McNeill, M.T. Alam, S. Lai, S. Sailer, V. Rauch, J. Patel, A. Hermetter, G. Golderer, S. Geley, G. Werner-Felmayer, R.S. Plumb, G. Astarita, M. Ralser, K.M. Channon, E.R. Werner, Tetrahydrobiopterin and alkylglycerol monooxygenase substantially alter the murine macrophage lipidome, Proc. Natl. Acad. Sci. U. S. A. 112 (2015) 2431–2436, https://doi.org/10.1073/pnas.1414887112.
[19] S. Marquet, B. Bucheton, C. Reymond, L. Argiro, S.H. El-Safi, M.M. Kheir, J.-P. Desvignes, C. Béroud, A. Mergani, A. Hammad, A.J. Dessein, Exome sequencing identifies two variants of the alkylglycerol monooxygenase gene as a cause of relapses in visceral Leishmaniasis in children, in Sudan, J. Infect. Dis. 216 (2017) 22–28, https://doi.org/10.1093/infdis/jix277.
[20] N. Alrayes, H.S.A. Mohamoud, S. Ahmed, M.M. Almramhi, T.M. Shuaib, J. Wang, J. Y. Al-Aama, K. Everett, J. Nasir, M. Jelani, The alkylglycerol monooxygenase (AGMO) gene previously involved in autism also causes a novel syndromic form of primary microcephaly in a consanguineous Saudi family, J. Neurol. Sci. 363 (2016) 240–244, https://doi.org/10.1016/j.jns.2016.02.063.
[21] V. Okur, K. Watschinger, D. Niyazov, J. McCarrier, D. Basel, M. Hermann, E. R. Werner, W.K. Chung, Biallelic variants in AGMO with diminished enzyme activity are associated with a neurodevelopmental disorder, Hum. Genet. 138 (2019) 1259–1266, https://doi.org/10.1007/s00439-019-02065-x.
[22] J. Sebat, B. Lakshmi, D. Malhotra, J. Troge, C. Lese-Martin, T. Walsh, B. Yamrom, S. Yoon, A. Krasnitz, J. Kendall, A. Leotta, D. Pai, R. Zhang, Y.-H. Lee, J. Hicks, S. J. Spence, A.T. Lee, K. Puura, T. Lehtimäki, D. Ledbetter, P.K. Gregersen, J. Bregman, J.S. Sutcliffe, V. Jobanputra, W. Chung, D. Warburton, M.-C. King, D. Skuse, D.H. Geschwind, T.C. Gilliam, K. Ye, M. Wigler, Strong association of de novo copy number mutations with autism, Science 316 (2007) 445–449, https://doi.org/10.1126/science.1138659.
[23] K.A. Fakhro, M. Choi, S.M. Ware, J.W. Belmont, J.A. Towbin, R.P. Lifton, M. K. Khokha, M. Brueckner, Rare copy number variations in congenital heart disease patients identify unique genes in left-right patterning, Proc. Natl. Acad. Sci. U. S. A. 108 (2011) 2915–2920, https://doi.org/10.1073/pnas.1019645108.
[24] S. Sailer, M.A. Keller, E.R. Werner, K. Watschinger, The emerging physiological role of AGMO 10 years after its gene identification, Life. 11 (2021), https://doi.org/10.3390/life11020088.
[25] S. Sailer, S. Coassin, K. Lackner, C. Fischer, E. McNeill, G. Streiter, C. Kremser, M. Maglione, C.M. Green, D. Moralli, A.R. Moschen, M.A. Keller, G. Golderer, G. Werner-Felmayer, I. Tegeder, K.M. Channon, B. Davies, E.R. Werner, K. Watschinger, When the genome bluffs: a tandem duplication event during generation of a novel agmo knockout mouse model fools routine genotyping, Cell Biosci. 11 (2021) 54, https://doi.org/10.1186/s13578-021-00566-9.
[26] A. Gallego-García, A.J. Monera-Girona, E. Pajares-Martínez, E. Bastida-Martínez, R. Pérez-Castaño, A.A. Iniesta, M. Fontes, S. Padmanabhan, M. Elías-Arnanz, A bacterial light response reveals an orphan desaturase for human plasmalogen synthesis, Science 366 (2019) 128–132, https://doi.org/10.1126/science.aay1436.
[27] M. Wainberg, R.A. Kamber, A. Balsubramani, R.M. Meyers, N. Sinnott-Armstrong, D. Hornburg, L. Jiang, J. Chan, R. Jian, M. Gu, A. Shcherbina, M.M. Dubreuil, K. Spees, W. Meuleman, M.P. Snyder, M.C. Bassik, A. Kundaje, A genome-wide atlas of co-essential modules assigns function to uncharacterized genes, Nat. Genet. 53 (2021) 638–649, https://doi.org/10.1038/s41588-021-00840-z.
[28] J.K. White, A.-K. Gerdin, N.A. Karp, E. Ryder, M. Buljan, J.N. Bussell, J. Salisbury, S. Clare, N.J. Ingham, C. Podrini, R. Houghton, J. Estabel, J.R. Bottomley, D. G. Melvin, D. Sunter, N.C. Adams, , Sanger Institute Mouse Genetics Project, D. Tannahill, D.W. Logan, D.G. Macarthur, J. Flint, V.B. Mahajan, S.H. Tsang, I. Smyth, F.M. Watt, W.C. Skarnes, G. Dougan, D.J. Adams, R. Ramirez-Solis, A. Bradley, K.P. Steel, Genome-wide generation and systematic phenotyping of knockout mice reveals new roles for many genes, Cell 154 (2013) 452–464, https://doi.org/10.1016/j.cell.2013.06.022.
[29] W.C. Skarnes, B. Rosen, A.P. West, M. Koutsourakis, W. Bushell, V. Iyer, A. O. Mujica, M. Thomas, J. Harrow, T. Cox, D. Jackson, J. Severin, P. Biggs, J. Fu, M. Nefedov, P.J. de Jong, A.F. Stewart, A. Bradley, A conditional knockout resource for the genome-wide study of mouse gene function, Nature 474 (2011) 337–342, https://doi.org/10.1038/nature10163.
[30] A. Bradley, K. Anastassiadis, A. Ayadi, J.F. Battey, C. Bell, M.-C. Birling, J. Bottomley, S.D. Brown, A. Bürger, C.J. Bult, W. Bushell, F.S. Collins, C. Desaintes, B. Doe, A. Economides, J.T. Eppig, R.H. Finnell, C. Fletcher, M. Fray, D. Frendewey, R.H. Friedel, F.G. Grosveld, J. Hansen, Y. Hérault, G. Hicks, A. Hörlein, R. Houghton, M.Hrabé de Angelis, D. Huylebroeck, V. Iyer, P.J. de Jong, J.A. Kadin, C. Kaloff, K. Kennedy, M. Koutsourakis, K.C.K. Lloyd, S. Marschall, J. Mason, C. McKerlie, M.P. McLeod, H. von Melchner, M. Moore, A. O. Mujica, A. Nagy, M. Nefedov, L.M. Nutter, G. Pavlovic, J.L. Peterson, J. Pollock, R. Ramirez-Solis, D.E. Rancourt, M. Raspa, J.E. Remacle, M. Ringwald, B. Rosen, N. Rosenthal, J. Rossant, P.Ruiz Noppinger, E. Ryder, J.Z. Schick, F. Schnütgen, P. Schofield, C. Seisenberger, M. Selloum, E.M. Simpson, W.C. Skarnes, D. Smedley, W.L. Stanford, A.F. Stewart, K. Stone, K. Swan, H. Tadepally, L. Teboul, G. P. Tocchini-Valentini, D. Valenzuela, A.P. West, K.-I. Yamamura, Y. Yoshinaga, W. Wurst, The mammalian gene function resource: the International Knockout Mouse Consortium, Mamm. Genome 23 (2012) 580–586, https://doi.org/10.1007/s00335-012-9422-2.
[31] S.J. Pettitt, Q. Liang, X.Y. Rairdan, J.L. Moran, H.M. Prosser, D.R. Beier, K.C. Lloyd, A. Bradley, W.C. Skarnes, Agouti C57BL/6N embryonic stem cells for mouse genetic resources, Nat. Methods 6 (2009) 493–495, https://doi.org/10.1038/nmeth.1342.
[32] N.J. Ingham, S.A. Pearson, V.E. Vancollie, V. Rook, M.A. Lewis, J. Chen, A. Buniello, E. Martelletti, L. Preite, C.C. Lam, F.D. Weiss, Z. Powis, P. Suwannarat, C.J. Lelliott, S.J. Dawson, J.K. White, K.P. Steel, Mouse screen reveals multiple new genes underlying mouse and human hearing loss, PLoS Biol. 17 (2019), e3000194, https://doi.org/10.1371/journal.pbio.3000194.
[33] J. Koch, K. Lackner, Y. Wohlfarter, S. Sailer, J. Zschocke, E.R. Werner, K. Watschinger, M.A. Keller, Unequivocal mapping of molecular ether lipid species by LC-MS/MS in plasmalogen-deficient mice, Anal. Chem. 92 (2020) 11268–11276, https://doi.org/10.1021/acs.analchem.0c01933.
[34] F.M. Vaz, J.H. McDermott, M. Alders, S.B. Wortmann, S. Kölker, M.L. Pras-Raves, M.A.T. Vervaart, H. van Lenthe, A.C.M. Luyf, H.L. Elfrink, K. Metcalfe, S. Cuvertino, P.E. Clayton, R. Yarwood, M.P. Lowe, S. Lovell, R.C. Rogers, Deciphering Developmental Disorders Study, A.H.C. van Kampen, J.P.N. Ruiter, R. J.A. Wanders, S. Ferdinandusse, M. van Weeghel, M. Engelen, S. Banka, Mutations in PCYT2 disrupt etherlipid biosynthesis and cause a complex hereditary spastic paraplegia, Brain 142 (2019) 3382–3397, https://doi.org/10.1093/brain/awz291.
[35] E.R. Werner, M.A. Keller, S. Sailer, D. Seppi, G. Golderer, G. Werner-Felmayer, R. A. Zoeller, K. Watschinger, A novel assay for the introduction of the vinyl ether double bond into plasmalogens using pyrene-labeled substrates, J. Lipid Res. 59 (2018) 901–909, https://doi.org/10.1194/jlr.d080283.
[36] K. Watschinger, E.R. Werner, Alkylglycerol monooxygenase, IUBMB Life 65 (2013) 366–372, https://doi.org/10.1002/iub.1143.
[37] L.-C. Wu, D.R. Pfeiffer, E.A. Calhoon, F. Madiai, G. Marcucci, S. Liu, M. S. Jurkowitz, Purification, identification, and cloning of lysoplasmalogenase, the enzyme that catalyzes hydrolysis of the vinyl ether bond of lysoplasmalogen, J. Biol. Chem. 286 (2011) 24916–24930, https://doi.org/10.1074/jbc.M111.247163.
[38] J. Koch, K. Watschinger, E.R. Werner, M.A. Keller, Tricky isomers-the evolution of analytical strategies to characterize plasmalogens and plasmanyl ether lipids, Front. Cell Dev. Biol. 10 (2022), 864716, https://doi.org/10.3389/fcell.2022.864716.
[39] N. Jiménez-Rojo, M.D. Leonetti, V. Zoni, A. Colom, S. Feng, N.R. Iyengar, S. Matile, A. Roux, S. Vanni, J.S. Weissman, H. Riezman, Conserved functions of ether lipids and sphingolipids in the early secretory pathway, Curr. Biol. 30 (2020) 3775–3787.e7, https://doi.org/10.1016/j.cub.2020.07.059.
[40] F. Dorninger, A. Brodde, N.E. Braverman, A.B. Moser, W.W. Just, S. Forss-Petter, B. Brügger, J. Berger, Homeostasis of phospholipids - the level of phosphatidylethanolamine tightly adapts to changes in ethanolamine plasmalogens, Biochim. Biophys. Acta 2015 (1851) 117–128, https://doi.org/10.1016/j.bbalip.2014.11.005.
[41] M. Honsho, F. Dorninger, Y. Abe, D. Setoyama, R. Ohgi, T. Uchiumi, D. Kang, J. Berger, Y. Fujiki, Impaired plasmalogen synthesis dysregulates liver X receptor-dependent transcription in cerebellum, J. Biochem. (2019), https://doi.org/10.1093/jb/mvz043.
[42] M.A. Surma, M.J. Gerl, R. Herzog, J. Helppi, K. Simons, C. Klose, Mouse lipidomics reveals inherent flexibility of a mammalian lipidome, Sci. Rep. 11 (2021) 1–14, https://doi.org/10.1038/s41598-021-98702-5.
[43] D. Fitzner, J.M. Bader, H. Penkert, C.G. Bergner, M. Su, M.-T. Weil, M.A. Surma, M. Mann, C. Klose, M. Simons, Cell-type- and brain-region-resolved mouse brain

lipidome, Cell Rep. 32 (2020), 108132, https://doi.org/10.1016/j.celrep.2020.108132.
[44] L. Liaw, I. Prudovsky, R.A. Koza, R.V. Anunciado-Koza, M.E. Siviski, V. Lindner, R. E. Friesel, C.J. Rosen, P.R.S. Baker, B. Simons, C.P.H. Vary, Lipid profiling of in vitro cell models of adipogenic differentiation: relationships with mouse adipose tissues, J. Cell. Biochem. 117 (2016) 2182–2193, https://doi.org/10.1002/jcb.25522.
[45] A.R. Malheiro, T.F. da Silva, P. Brites, Plasmalogens and fatty alcohols in rhizomelic chondrodysplasia punctata and Sjögren-Larsson syndrome, J. Inherit. Metab. Dis. 38 (2015) 111–121, https://doi.org/10.1007/s10545-014-9795-3.